RAPID COMMUNICATIONS

PHYSICAL REVIEW A **91**, 041401(R) (2015)

Light shifts in a pulsed cold-atom coherent-population-trapping clock

E. Blanshan,[1] S. M. Rochester,[2] E. A. Donley,[1,*] and J. Kitching[1]

[1]*National Institute of Standards and Technology, Boulder, Colorado 80305, USA*

[2]*Rochester Scientific, LLC, El Cerrito, California 94530, USA*

(Received 16 October 2014; published 10 April 2015)

Field-grade atomic clocks capable of primary standard performance in compact physics packages would be of significant value in applications ranging from network synchronization to inertial navigation. A coherent-population-trapping clock featuring laser-cooled ^{87}Rb atoms and pulsed Ramsey interrogation is a strong candidate for this technology if the frequency biases can be minimized and controlled. Here we characterize the light shift in a cold-atom coherent-population-trapping clock, explaining observed shifts in terms of phase shifts that arise during the formation of dark-state coherences combined with optical-pumping effects caused by unwanted incoherent light in the interrogation spectrum. Measurements are compared with existing and new theoretical treatments, and a laser configuration is identified that would reduce clock frequency uncertainty from light shifts to a fractional frequency level of $\Delta\nu/\nu = 4 \times 10^{-14}$ per 100 kHz of laser frequency uncertainty.

DOI: 10.1103/PhysRevA.91.041401 PACS number(s): 32.60.+i, 06.30.Ft, 42.62.Fi

New technologies for high-performance compact atomic clocks capable of field operation have been investigated from multiple directions in recent years. Portable ion clocks based on Hg [1] and Yb [2] are candidate technologies as are neutral-atom clocks based on microwave cavities [3,4] or coplanar waveguides [5]. Chip-scale atomic clocks (CSACs) based on microfabricated vapor cells [6,7] have already been integrated into applications where size and power restrictions preclude the use of conventional frequency references. CSACs rely on coherent population trapping (CPT) [8–11] to interrogate microwave transitions optically, eliminating the need for large microwave cavities. Although CSACs can provide fractional frequency stabilities at 1 s of integration that are below 1×10^{-10}, changing pressure shifts from the high-pressure buffer gas and light shifts from the interrogation light introduce frequency drifts that limit the long-term stability. These drifts can be eliminated by generating long CPT interactions with laser-cooled atoms [12] in lieu of buffer gases, potentially enabling fundamentally accurate compact atomic clocks.

Earlier work demonstrated a cold-atom CPT (CACPT) clock with a fractional frequency stability of $\sim 4 \times 10^{-11}$ at 1 s of integration that mitigated Doppler shifts by probing the atoms with balanced counterpropagating CPT beams [13]. This configuration minimizes phase shifts accumulated due to the motion of the atoms during the interrogation sequence. Despite operating outside of the Lamb-Dicke regime [14], residual first-order Doppler shifts due to gravitational acceleration should be suppressed below 10^{-13} for a balanced horizontal CPT field [13].

Minimizing light shifts [15–18] is also critical as they can be a main frequency bias in CPT clocks. Light shifts can be made smaller when the atoms are probed with pulsed Ramsey interrogation using pump and probe light pulses as opposed to probing continuously. The light shift for Ramsey interrogation has been previously studied in a sodium beam clock [19–22] as well as in vapor-cell clocks [23,24]. The dominant light shift for Raman-Ramsey interactions behaves fundamentally differently from the well-known ac Stark shift that arises when the energy levels of polarizable atoms are shifted by harmonic electric fields [25]. In contrast, the light shift in Raman-Ramsey interactions depends only on the parameters of the CPT light that affect the rate of dark-state formation during the first Ramsey pulse. The light shift vanishes in the limit of sufficiently large intensity and duration for the first (pump) pulse. Low-intensity and/or detuned CPT light fields, however, generate low excitation rates such that the atoms are not completely transferred to the dark state during the finite length of the first pulse. The resulting shift scales inversely with the Ramsey period T_R and changes sign depending on the initial hyperfine ground state F_0 [20]. The shift is also largely insensitive to the intensity ratio of the two laser frequencies that excite the dark state as long as the total intensity is constant. Because of its association with the coherence terms in the density-matrix formalism, we refer to this shift as the coherent light shift throughout this Rapid Communication.

The measured light shifts in our Raman-Ramsey CPT clock do not vanish at high intensity as predicted by the established theory for the coherent shift [20]. The residual shifts at high intensities scale as T_R^{-1} but are independent of laser intensity, pump pulse duration, and initial hyperfine level.

In this study, we show that the residual shift can be explained by a dynamic equilibrium driven by optical pumping in which atoms continuously scatter out of and reenter the dark state. This precludes the formation of a complete dark state with the precise optical phase of the CPT laser field, causing potentially large residual shifts. In our system, this optical pumping results from a pedestal of incoherent light surrounding the CPT frequency component that originates from our slave laser. This residual frequency noise on the slave laser is present because of bandwidth limitations of our optical phase-locked loop (PLL) that we use to generate the CPT spectrum. Similar shifts can be expected in any system in which decay of the dark state results in a change in the initial-state population.

Our system combines lin||lin CPT [26–29] with laser-cooled atoms and pulsed Ramsey interrogation [12,19,23,24,30–38]. In lin||lin CPT [Fig. 1(a)], a bichromatic field with parallel linear polarizations and frequencies separated by the 6.835-GHz ground-state hyperfine splitting in

*elizabeth.donley@nist.gov

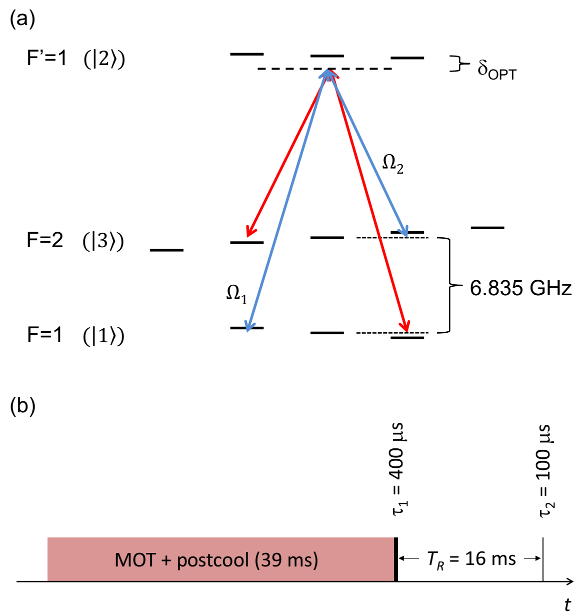

FIG. 1. (Color online) (a) Energy levels in the lin||lin CPT configuration for ^{87}Rb (not to scale). Two independent Λ systems are shown (red and blue arrows). Labels in parentheses identify states of the three-level system used in the theory below. The Rabi frequencies of the light connecting $|F=1,2\rangle \to |F=1'\rangle$ are Ω_1 and Ω_2, respectively. (b) A typical single Ramsey sequence. The widths of the magneto-optical trap (MOT), pump, Ramsey, and probe pulses are to scale with typical operating parameters.

^{87}Rb couples atoms into a double-Λ system connecting the $|F=1,m_F=\pm1\rangle$ and $|F=2,m_F=\mp1\rangle$ ground states via the $5\,^2P_{1/2}$, $|F'=1,m_F=0\rangle$ level. Unlike conventional CPT configurations, the lin||lin scheme does not have trap states and exhibits an improved resonance contrast. Although the individual Λ systems are not true clock transitions and are sensitive to Zeeman shifts, the first-order Zeeman shifts cancel if the transition amplitudes are balanced.

The CPT light is generated by phase locking two megahertz linewidth 795-nm laser diodes. In our standard configuration, the master laser is a distributed Bragg reflector laser that is locked to the $|F=2\rangle \to |F'=1\rangle$ transition by saturated absorption spectroscopy. The slave is a distributed feedback laser that is tuned to the $|F=1\rangle \to |F'=1\rangle$ transition by a PLL. The offset frequency between the master and the slave lasers is referenced to a Cs beam clock such that absolute frequency shifts from the ^{87}Rb ground-state hyperfine splitting can be measured.

The two CPT beams are overlapped and coupled into a single-mode polarization-maintaining fiber with a 3.8 mm e^{-2} diameter output beam. The CPT light passes horizontally through the atoms and is retroreflected in the Doppler-suppressed standing-wave configuration [13].

The atom source is a MOT with a 35-ms cooling period and 10 mW of cooling light, which enters the system via a three-way fiber splitter with 3.8 mm e^{-2} diameter output beams, typically trapping 2×10^5 atoms. During a postcool stage, the laser detuning is ramped by -8γ (γ = natural linewidth of ^{87}Rb), increasing the MOT recapture between clock cycles. A bias magnetic field of 4.5 μT is aligned along the propagation direction of the CPT beams.

A typical cycle for performing a single absorption measurement is shown in Fig. 1(b). The first CPT pulse of typical duration $\tau_1 = 400\ \mu$s pumps atoms into the dark state. After the Ramsey period of up to 16 ms, the accumulated phase shift between the dark state and the local oscillator is probed via the absorption during the leading edge of a second 100-μs CPT pulse. To perform a clock frequency measurement, the absolute frequency of the central Ramsey fringe is measured with a digital servo that alternately performs absorption measurements on opposite sides of the central Ramsey fringe by modulating the PLL offset frequency.

To evaluate the light shift, the clock frequency was measured versus total CPT-light intensity $I_{\rm CPT}$ for multiple optical detunings $\delta_{\rm opt}$ and varied τ_1, T_R, and F_0. To prepare the atoms in the $|F_0=1\rangle$ level, a 400-μs pulse from the MOT laser was applied after the postcool stage. Without this pulse, the $|F_0=2\rangle$ state is naturally populated by the cooling process.

Since the coherent shift arises when the duration of τ_1 is insufficient for the dark state to fully form, the shift magnitude depends critically on the dark-state loading rate. Mathematically, this behavior is described by an exponential in the observed phase shift [20],

$$\tan(\Delta\phi) \propto \left(\rho_{11}^0 - \rho_{33}^0\right)\exp(-\Omega^2 S\tau_1), \tag{1}$$

where $\rho_{11}^0 - \rho_{33}^0$ is the ground-state population difference and Ω is the average Rabi frequency for the two CPT frequency components. Following the notation of Ref. [20], the Raman damping rate is

$$\Omega^2 S = \Omega^2\gamma / \left(\gamma^2 + 4\delta_{\rm opt}^2\right). \tag{2}$$

The Raman saturation parameter is the product of the Raman damping rate and the length of the first Ramsey pulse τ_1. When $\Omega^2 S\tau_1 \gg 1$, the system nearly reaches an equilibrium dark state before the end of the pumping pulse, resulting in a minimal shift of the Ramsey fringes.

Light shifts for varied τ_1, T_R, and F_0 are shown in Figs. 2 and 3 versus $\Omega^2 S\tau_1$. The coherent light shift is visible for $\Omega^2 S\tau_1 \lesssim 10$ where a low Raman damping rate causes a significant phase shift that changes sign depending on F_0 (not shown). The shift flattens at high intensities and for long pulse durations, leaving a residual shift that is the dominant contribution to the overall frequency shift of the CPT clock from the absolute transition frequency. As seen in Fig. 2, the theoretical coherent shift does not capture the residual light shift at high intensities. We attribute the disagreement to the fact that the model does not take into account the effect of incoherent light present in the experiment.

The T_R^{-1} dependence of both the coherent and the residual contributions is shown in Fig. 3. For longer T_R, the same phase shift results in a smaller frequency shift owing to the reduced Fourier linewidth of the Ramsey fringes: $\Delta\nu_{LS} = \Delta\phi/(2\pi T_R)$.

The intensity-independent residual shift is proportional to the detuning, is independent of the initial hyperfine ground state, and in terms of fractional frequency is 10^{-10} per megahertz of optical detuning for $T_R = 16$ ms. A shift of this size would require laser frequency stabilization of $\sim$1 kHz to reduce it to the 10^{-13} level.

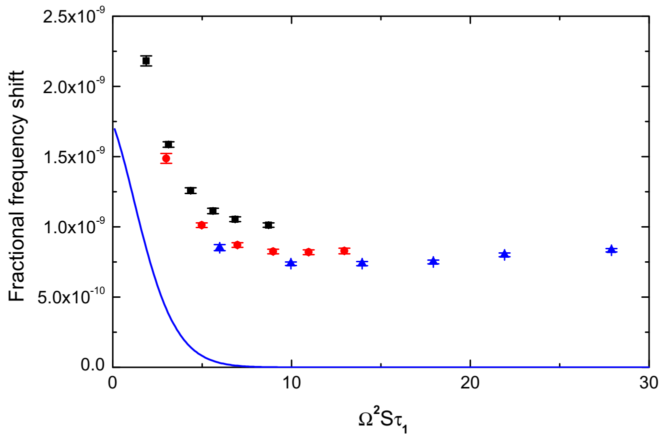

FIG. 2. (Color online) Measured clock frequency shift from the ^{87}Rb ground-state hyperfine splitting versus the Raman saturation parameter $\Omega^2 S\tau_1$ for three values of τ_1 (■: 250 μs; ●: 400 μs; ▲: 800 μs) and the theoretically predicted shift (line) [20]. The motivation for expressing the intensity in terms of $\Omega^2 S\tau_1$ is clear since data collected with three different values of τ_1 fall roughly on the same curve. Here, $\delta_{\rm opt} = 2$ MHz, $T_R = 4$ ms, and $F_0 = 1$. A Zeeman shift of 1.3×10^{-10} was subtracted from the data to account for the magnetic bias field. The theoretical model used here does not include scattering from incoherent light.

To directly compare the measured coherent shifts with the theory developed in Ref. [20], we removed the residual shift through linear combinations of measurements made for both hyperfine states. The sign of the coherent shift inverts between $|F_0 = 1,2\rangle$ [Eq. (1)], whereas the pumping-induced shift is equal for both. We can express the total shift for each case as $\delta\nu_i = \delta\nu_{Ci} + \delta\nu_p$, where $\delta\nu_i$ and $\delta\nu_{Ci}$ are the total and coherent shifts when atoms originate in the ith hyperfine state and $\delta\nu_p$ is the pumping-induced shift. The average coherent

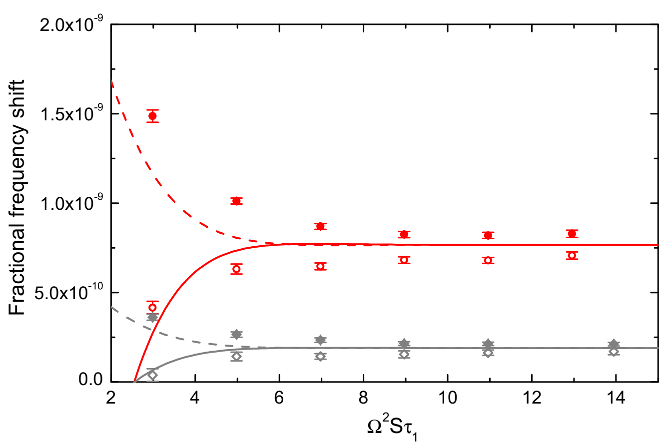

FIG. 3. (Color online) Measured clock frequency difference from the ^{87}Rb ground-state hyperfine splitting versus $\Omega^2 S\tau_1$ for varied F_0 (○◇: $|F_0 = 1\rangle$; ●◆: $|F_0 = 2\rangle$), and T_R (○●: $T_R = 4$ ms; ◇◆: $T_R = 16$ ms) with $\delta_{\rm opt} = 2$ MHz and $\tau_1 = 400$ μs. The theory curves (lines), calculated from Eqs. (4) and (5), incorporate incoherent pumping. A Zeeman shift of 1.3×10^{-10} was subtracted from the data to account for the magnetic bias field. Observed light shifts are equal and opposite for negative detunings.

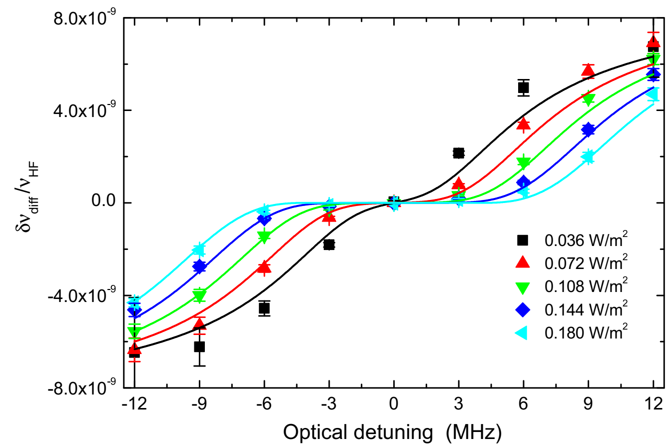

FIG. 4. (Color online) Comparison of coherent light shifts measured for different $I_{\rm CPT}$ values (points) to the full theoretical model (lines) [20] for $T_R = 4$ ms and $\tau_1 = 400$ μs.

shift can then be found with the linear combination,

$$\overline{\delta\nu}_{CF12} = \tfrac{1}{2}(\delta\nu_2 - \delta\nu_1) = \tfrac{1}{2}(\delta\nu_{C2} + |\delta\nu_{C1}|) \equiv \delta\nu_{\rm diff}. \quad (3)$$

Theory curves for $\delta\nu_{\rm diff}$ generated using the full formalism in Ref. [20] are compared to our measurements in Fig. 4. Excellent quantitative agreement is demonstrated with no adjustable parameters.

Although the coherent shift agrees well with theoretical expectations, the intensity-independent residual shift deviates from dependences typical of light-shift effects. We attribute the residual shift to optical pumping from incoherent light. Delayed self-heterodyne measurements of the laser spectra have shown that the slave is the dominant source of incoherent light. The dark state is not transparent to this incoherent light because of its random phase. With the lasers in what we define as Configuration 1 (see Fig. 6), this incoherent light is resonant with the $|F = 1\rangle \rightarrow |F' = 1\rangle$ transition. Atoms that scatter out of the dark state are preferentially pumped to $|F = 2\rangle$ from which they reenter the dark state. This establishes a dynamic equilibrium during τ_1 in which atoms continuously leave and reenter the dark state.

This pumping cycle modifies the dark-state loading process such that regardless of the duration of τ_1, the complete dark state is never formed. Equilibrium consists of a dark state with a population and average phase that depends critically on the fraction of coherent light in the CPT spectrum $P_{\rm carrier}$. This is illustrated in Fig. 5(a) where the dependence of the pumping-induced residual shift on $P_{\rm carrier}$ is shown, demonstrating that suppression of the shift is possible if the performance of the PLL is improved.

An optimized beat note between master and slave lasers is shown in Fig. 5(b). We typically obtain a fractional power in the coherent carrier of 0.73, corresponding to a phase error variance of $\sigma_\phi^2 = 0.35$ rad^2 when integrated over 20 MHz [39].

To theoretically model the optical pumping induced light shift, we modified the framework developed in Ref. [20] for a three-level system that ignores Zeeman sublevels. This approach uses the density operator master equation [40] that was applied to a three-level system in Ref. [41]. To simplify the modeling of the incoherent light, we treat scattering from

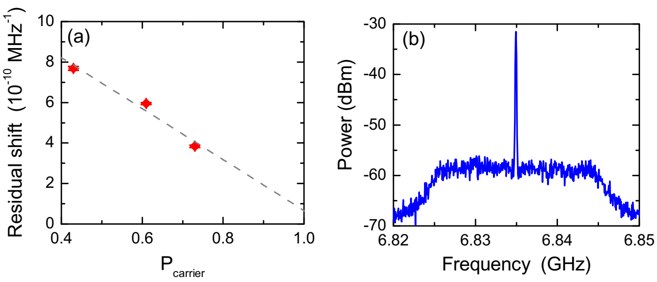

FIG. 5. (Color online) (a) Pumping-induced light shift versus P_{carrier} for $T_R = 4$ ms. P_{carrier} was adjusted by deoptimizing the PLL settings. Given the fitting error, the linear fit is consistent with zero for 100% carrier power as would be predicted by Eq. (4). (b) Beat note between master and slave lasers with $P_{\text{carrier}} = 0.73$. (Resolution bandwidth = 100 kHz.)

incoherent light in an analogous way to spontaneous decay [42]. Incoherent light couplings are parametrized by β_{12} and β_{32}, the incoherent scattering rate between the $|F = 1,2\rangle \rightarrow |F' = 1\rangle$ levels, respectively. The density-matrix equations governing the system become

$$
\begin{aligned}
\dot{\rho_{11}} &= \frac{i}{2}(-\Omega_1\alpha_{12} + \Omega_1^*\alpha_{12}^*) + \Gamma_{21}\rho_{22} - \beta_{12}\rho_{11},\\
\dot{\rho_{22}} &= \frac{i}{2}(\Omega_1\alpha_{12} - \Omega_1^*\alpha_{12}^* + \Omega_2\alpha_{32} - \Omega_2^*\alpha_{32}^*) - \gamma\rho_{22}\\
&\quad + \beta_{12}\rho_{11} + \beta_{32}\rho_{33},\\
\dot{\rho_{33}} &= \frac{i}{2}(-\Omega_2\alpha_{32} + \Omega_2^*\alpha_{32}^*) + \Gamma_{23}\rho_{22} - \beta_{32}\rho_{33},\\
\dot{\alpha_{12}} &= \frac{i}{2}\Omega_1^*(\rho_{22} - \rho_{11}) - \frac{i}{2}\Omega_2^*\alpha_{13} - \frac{1}{2}(\gamma + 2i\delta_1 + \beta_{12})\alpha_{12},\\
\dot{\alpha_{32}} &= \frac{i}{2}\Omega_2^*(\rho_{22} - \rho_{33}) - \frac{i}{2}\Omega_1^*\alpha_{13}^* - \frac{1}{2}(\gamma + 2i\delta_2 + \beta_{32})\alpha_{32},\\
\dot{\alpha_{13}} &= \frac{i}{2}(\Omega_1^*\alpha_{32}^* - \Omega_2\alpha_{12}) - i(\delta_1 - \delta_2)\alpha_{13}\\
&\quad - \frac{1}{2}(\beta_{12} + \beta_{32})\alpha_{13}.
\end{aligned}
\tag{4}
$$

The rotating-wave and electric dipole approximations are assumed, the indices 1, 2, and 3 correspond to the $|F = 1\rangle$, $|F' = 1\rangle$, and $|F = 2\rangle$ states, respectively, ρ_{ii} is the population density, α_{ij} is the coherence, Γ_{ij} is the decay rate between levels i and j, and $\delta_{1,2}$ is the detuning of the CPT frequency components.

The incoherent scattering rates are given by the convolution of the natural (Lorentzian) line-shape function with the spectral line-shape function of the incoherent light. Assuming the incoherent light has a flat spectrum of width Δ_{ic} and assuming it is centered on the optical resonance, we find

$$
\beta_{ij} = \int_{-\Delta_{ic}/2}^{+\Delta_{ic}/2} \frac{\epsilon\Omega_{ic}^2}{\Delta_{ic}} \frac{\gamma}{\gamma^2 + 4\delta^2} d\delta = \epsilon\Omega_{ic}^2 \frac{\arctan\, \Delta_{ic}/\gamma}{\Delta_{ic}}, \tag{5}
$$

where Ω_{ic} is the Rabi frequency of the incoherent light that would be induced by resonant narrow-band light of the same power as the total integrated incoherent light power and ϵ is a scaling factor. This expression is derived from the standard

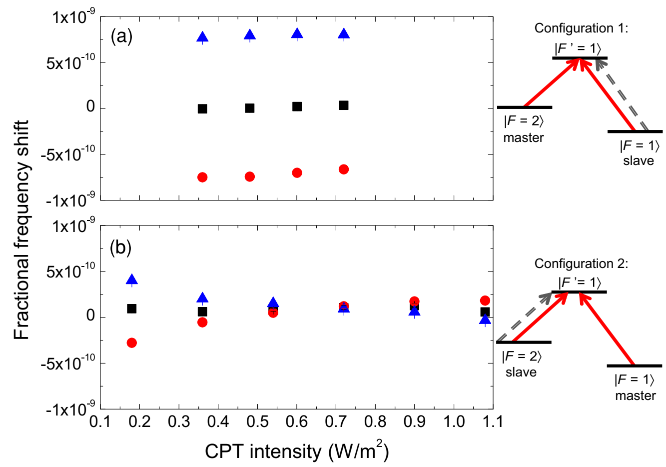

FIG. 6. (Color online) Light shifts for three different values of the δ_{opt} (■: 0 MHz; ●: -2 MHz ▲: $+2$ MHz) with $T_R = 4$ ms and $F_0 = 1$. Data are shown with the laser system in (a) Configuration 1 and (b) Configuration 2 with the corresponding laser configurations shown to the right of the plots.

two-level scattering rate in the intensity regime in which the clock operates ($\Omega \ll \gamma$). Terms in Eq. (4) corresponding to stimulated emission from incoherent light are small relative to Γ_{21} and Γ_{23} and are neglected.

The density-matrix equations above are numerically solved under the assumption of a closed three-level system, which has been shown to provide reasonable agreement in past experiments [20]. We also assume a short-lived excited state $\Omega_1 = \Omega_2$ and $\delta_1 = \delta_2$. The coherent phase shift is calculated from $\tan(\phi) = \text{Im}[\alpha_{13}(\tau_1)]/\text{Re}[\alpha_{13}(\tau_1)]$. The β_{ij} parameter is evaluated by integrating a white-noise spectrum with an intensity given by $(1 - P_{\text{carrier}})I_{\text{CPT}}$ spread over a 16-MHz-wide band centered on the coherent carrier.

Modeled light shifts exhibit the qualitative behavior observed in the data, showing no dependence on τ_1, F_0, or intensity at large I_{CPT}. These calculations agree with our data quantitatively with the addition of a scaling factor of $\epsilon = 2.7$ (applied in Fig. 3). This discrepancy in the incoherent light intensity needed to fit the data may result from simplifications in the calculation listed above as well as the approximations that were made to account for the incoherent light in the model. These approximations dramatically simplify the calculations; a thorough multilevel treatment accounting for these effects would be expected to give better quantitative agreement with experimental data.

The detuning dependence of the pumping-induced light shift is determined by the level to which atoms are pumped after scattering out of the dark state, which we have confirmed by exchanging the roles of the master and slave lasers (Fig. 6). For laser Configuration 1, atoms preferentially reenter the dark state from $|F = 2\rangle$, and the pumping-induced shift exhibits a detuning dependence with the same sign as the coherent shift for atoms with $|F_0 = 2\rangle$. To verify this behavior, the frequencies of the master and slave lasers were exchanged, placing the laser system in Configuration 2. The incoherent light now drives optical pumping to the $|F = 1\rangle$ level, inverting the detuning dependence of the residual shift at high I_{CPT}.

The magnitude of the observed pumping-induced shift at high intensities in Configuration 2 is suppressed over Configuration 1 by a factor of ~ 6. We attribute this reduction to the smaller number of Zeeman sublevels in $|F = 1\rangle$. Atoms accumulating in $|F = 2\rangle$ (Configuration 1) decay into one of five m_F levels, three of which are not in the double-Λ system and require additional excitation cycles before reentering the dark state. For Configuration 2, atoms accumulate in the three m_F levels of $|F = 1\rangle$ where the time required to repump into the dark state is reduced, suppressing the pumping-induced shift. Measurements of the $|F_0 = 1\rangle$ coherent shift are consistently smaller than the corresponding shift for the $|F_0 = 2\rangle$ case due to the same effect, which is visible in the data in Fig. 3.

Locking the slave laser to the $|F = 2\rangle \to |F' = 1\rangle$ line also introduces a CPT intensity where the detuning dependence of the light shift vanishes. This zero crossing is caused by the inverted detuning dependence between the coherent shift at low intensities and the residual shift at higher intensities. The transition occurs very near the value of I_{CPT} that maximizes the fringe signal-to-noise ratio. Operating at the crossover point, we estimate a bound on the detuning dependence on the fractional clock frequency of 4×10^{-14} for 100 kHz of optical detuning for $T_R = 16$ ms. This is well below requirements for most applications.

The light shift, initially a concern for cold-atom clocks based on CPT, has been shown to be a technical concern that can be mitigated through attention to the PLL spectrum. We have characterized the light shift in our CACPT clock, including contributions from the coherent shift that is present only during formation of the atomic coherences and a shift arising from optical pumping by incoherent light. Careful measurements of the shifts agree well with our modeling, which was based on an existing model [20] that we expanded to account for scattering from incoherent light. We have also demonstrated a laser configuration in which shifts in the intensity regime relevant for clock operation should be suppressed at the 10^{-14} level. At this level of sensitivity, light shifts would not be a fundamental limit for a compact CACPT atomic clock.

Note added. Recent related research comparing light shifts modeled with and without the adiabatic approximation used in the derivation of Eq. (1) has been reported [43].

D. Budker, F.-X. Esnault, N. Ashby, G. Pati, E. Ivanov, S. Riedl, K. Beloy, and N. Abrams are gratefully acknowledged for technical help and discussions. This work is funded by NIST and the Defense Advanced Research Projects Agency (DARPA). NIST is an agency of the U.S. government, and this work is not subject to copyright. The views, opinions, and/or findings contained in this article are those of the authors and should not be interpreted as representing the official views or policies, either expressed or implied, of DARPA or the Department of Defense. (Approved for public release by DARPA, distribution unlimited.)

[1] J. D. Prestage, S. K. Chung, R. J. Thompson, and P. MacNeal, in *IEEE International Frequency Control Symposium, 2009 Joint with the 22nd European Frequency and Time Forum, Besançon, France, 2009* (IEEE, Piscataway, NJ, 2009), p. 54.
[2] Y.-Y. Jau, H. Partner, P. D. D. Schwindt, J. D. Prestage, J. R. Kellogg, and N. Yu, Appl. Phys. Lett. **101**, 253518 (2012).
[3] F.-X. Esnault, D. Holleville, N. Rossetto, S. Guerandel, and N. Dimarcq, Phys. Rev. A **82**, 033436 (2010).
[4] S. T. Muller, D. V. Magalhaes, R. F. Alves, and V. S. Bagnato, J. Opt. Soc. Am. B **28**, 2592 (2011).
[5] F. Ramirez-Martinez, C. Lacrote, P. Rosenbusch, F. Reinhard, C. Deutsch, T. Schneider, and J. Reichel, Adv. Space Res. **47**, 247 (2011).
[6] S. Knappe, V. Shah, P. D. D. Schwindt, L. Hollberg, J. Kitching, L.-A. Liew, and J. Moreland, Appl. Phys. Lett. **85**, 1460 (2004).
[7] R. Lutwak, P. Vlitas, M. Varghese, M. Mescher, D. K. Serkland, and G. M. Peake, in *Proceedings of the 2005 IEEE International Frequency Control Symposium, Vancouver, 2005* (IEEE, Piscataway, NJ, 2005), p. 752.
[8] G. Alzetta, A. Gozzini, L. Moi, and G. Orriols, Nuovo Cimento Soc. Ital. Fis., B **36**, 5 (1976).
[9] E. Arimondo, Prog. Opt. **35**, 257 (1996).
[10] J. Vanier, Appl. Phys. B **81**, 421 (2005).
[11] V. Shah and J. Kitching, Adv. At., Mol., Opt. Phys. **59**, 21 (2010).
[12] X. Chen, G.-Q. Yang, M.-S. Wang, and J. Zhan, Chin. Phys. Lett. **27**, 113201 (2010).
[13] F.-X. Esnault, E. Blanshan, E. N. Ivanov, R. E. Scholten, J. Kitching, and E. A. Donley, Phys. Rev. A **88**, 042120 (2013).
[14] R. H. Dicke, Phys. Rev. **89**, 472 (1953).
[15] G. Orriols, Nuovo Cimento Soc. Ital. Fis., B **53**, 1 (1979).
[16] J. P. Barrat and C. Cohen-Tannoudji, J. Phys. Radium **22**, 329 (1961).
[17] B. S. Mathur, H. Tang, and W. Happer, Phys. Rev. **171**, 11 (1968).
[18] C. Cohen-Tannoudji and J. Dupont-Roc, Phys. Rev. A **5**, 968 (1972).
[19] P. R. Hemmer, G. P. Ontai, and S. Ezekiel, J. Opt. Soc. Am. B **3**, 219 (1986).
[20] P. R. Hemmer, M. S. Shahriar, V. D. Natoli, and S. Ezekiel, J. Opt. Soc. Am. B **6**, 1519 (1989).
[21] P. R. Hemmer and M. Prentiss, J. Opt. Soc. Am. B **5**, 1613 (1988).
[22] M. S. Shahriar, P. R. Hemmer, D. P. Katz, A. Lee, and M. G. Prentiss, Phys. Rev. A **55**, 2272 (1997).
[23] T. Zanon-Willette, E. de Clercq, and E. Arimondo, Phys. Rev. A **84**, 062502 (2011).
[24] N. Castagna, R. Boudot, S. Guèrandel, E. de Clercq, N. Dimarcq, and A. Clairon, IEEE Trans. Ultrason. Ferroelectr. Freq. Control **56**, 246 (2009).
[25] J. Vanier and C. Audoin, *The Quantum Physics of Atomic Frequency Standards* (IOP, Bristol, 1989).
[26] A. V. Taichenachev, V. I. Yudin, V. L. Velichansky, and S. A. Zibrov, JETP Lett. **82**, 398 (2005).
[27] E. Breschi, G. Kazakov, R. Lammegger, G. Mileti, B. Matisov, and L. Windholz, Phys. Rev. A **79**, 063837 (2009).

[28] S. A. Zibrov, I. Novikova, D. F. Phillips, R. L. Walsworth, A. S. Zibrov, V. L. Velichansky, A. V. Taichenachev, and V. I. Yudin, Phys. Rev. A **81**, 013833 (2010).

[29] E. E. Mikhailov, T. Horrom, N. Belcher, and, I. Novikova, J. Opt. Soc. Am. B **27**, 417 (2010).

[30] J. E. Thomas, P. R. Hemmer, S. Ezekiel, C. C. Leiby, Jr., R. H. Picard, and C. R. Willis, Phys. Rev. Lett. **48**, 867 (1982).

[31] P. R. Hemmer, S. Ezekiel, and C. C. Leiby, Jr., Opt. Lett. **8**, 440 (1983).

[32] P. R. Hemmer, M. S. Shahriar, H. Lamela-Rivera, S. P. Smith, B. E. Bernacki, and S. Ezekiel, J. Opt. Soc. Am. B **10**, 1326 (1993).

[33] T. Zanon, S. Guerandel, E. de Clercq, D. Holleville, N. Dimarcq, and A. Clairon, Phys. Rev. Lett. **94**, 193002 (2005).

[34] T. Zanon, S. Tremine, S. Guerandel, E. de Clercq, D. Holleville, N. Dimarcq, and A. Clairon, IEEE Trans. Instrum. Meas. **54**, 776 (2005).

[35] S. Guerandel, T. Zanon, N. Castagna, F. Dahes, E. de Clercq, N. Dimarcq, and A. Clairon, IEEE Trans. Instrum. Meas. **56**, 383 (2007).

[36] R. Boudot, S. Guerandel, E. de Clercq, N. Dimarcq, and A. Clairon, IEEE Trans. Instrum. Meas. **58**, 1217 (2009).

[37] X. Liu, J.-M. Merolla, S. Guerandel, E. de Clercq, and R. Boudot, Opt. Express **21**, 12451 (2013).

[38] J.-M. Danet, M. Lours, S. Guerandel, and E. de Clercq, IEEE Trans. Ultrason., Ferroelectr., Freq. Control **61**, 567 (2014).

[39] E. N. Ivanov, F.-X. Esnault, and E. A. Donley, Rev. Sci. Instrum. **82**, 083110 (2011).

[40] C. Cohen-Tannoudji, J. Dupont-Roc, and G. Grynberg, *Atom-Photon Interactions: Basic Processes and Applications* (Wiley-VCH, New York, 1998).

[41] M. Fleischhauer, A. Imamoglu, and J. P. Marangos, Rev. Mod. Phys. **77**, 633 (2005).

[42] E. Blanshan, Ph.D. thesis, University of Colorado, 2014.

[43] G. S. Pati, Z. Warren, N. Yu, and M. S. Shahriar, J. Opt. Soc. Am. B **32**, 388 (2015).